Efficient Characterization of Materials Using the Doppler Effect in Microwaves

Roman PINCHUK, Christoph SKLARCZYK, Michael KRÖNING,
Fraunhofer IZFP, Saarbrücken
Wolfgang J. PAUL, Saarland University, Saarland

Abstract. A large number of microwave sensors are available on the market today. Unfortunately, sensors of high quality are very expensive and tend to be stationary, making them unsuitable for integrating into an industrial process. Processing of microwave data is a challenging and complex task, and leads to high computational demands and increased processing time, so real-time quality control becomes virtually impossible. In this paper, we introduce a prototype system for nondestructive testing that utilizes moderately expensive continuous wave (CW) sensors. We exploit the physical phenomenon of the Doppler Effect to detect discontinuities in materials. We also propose an approach for fast measurements and data processing.

Motivation

Use of inexpensive and primitive sensors for microwave NDT may significantly reduce the amount of information acquired about an object or even make the testing impossible. Often, the lack of information may be compensated through excessive data acquisition processes, after which the measured data are processed using signal processing algorithms. Usually, algorithms that deal with a large amount of data are computationally complex; this leads to a high level of computational strain and increased processing time so that real-time quality control becomes impractical. One idea is the development of a prototype system for efficient nondestructive testing based on continuous wave (CW) radar technology. Our definition of term efficient is a system which is chip based and permits fast measurement and data processing.

1. Physical Basics

1.1 CW-Radar principle

A time-varying signal (s^{in}) is applied to the input of the radar. This causes the activation of an electromagnetic field $E^{in}(\vec{r},t)$, which is defined at the spatial position ($\vec{r}$) and time (t). The field $E^{in}(\vec{r},t)$ propagates towards the object to be controlled and interacts with it. This interaction establishes the reflected electromagnetic field $E^{sc}(\vec{r},t)$, which propagates back to the radar. While the radar is receiving the scattered field $E^{sc}(\vec{r},t)$, it excites the time-varying signal (s^{sc}). According to the physical principles the CW radar produces an output signal (s^{out}) by combining both incident (s^{in}) and scattered (s^{sc}) signals:

$$s^{out}(t)=\left(s^{in}(t)+s^{sc}(t)\right)^2. \tag{1.1}$$

For the CW radar the incident signal is defined as:

$$s^{in}(t)=A^{in}\cos\left(2\pi f^{in}t+\varphi^{in}\right)$$

In equation (1.1) the amplitude (A^{in}) is proportional to the intensity of the incident electric field (E^{in}).The transmission frequency and the initial phase are $f^{in}=24\,\text{GHz}$ and φ^{in} respectively. The scatter signal (s^{sc})depends on the properties of the target. In the case of CW radar, only the output signal (s^{out}) can be measured. This signal is used for material characterization, i.e. flaw detection and evaluation.

1.2 Doppler Effect in microwaves

In order to measure the Doppler Effect in microwaves, CW radars were invented. The basic principle of the Doppler Effect in microwaves is presented in Figure 1.1.

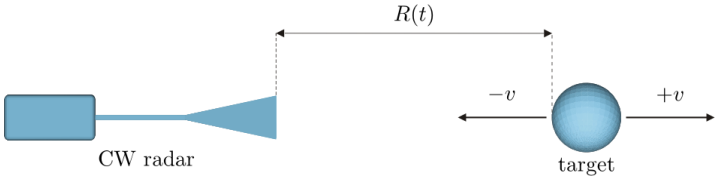

Figure 1.1: Schematic of the Doppler Experiment

The CW radar does not change its position, whereas the target moves. We define the speed of the target (v) to be a constant.

This ensures the linear increase or decrease of the distance (R) between the radar and the target in time:

$$R(t)=R_0\pm v(t-t_0), \tag{1.2}$$

Where t_0 is an initial time, R_0 is the initial radar-target distance. In equation (1.2), the approaching of the target is given by a "minus" sign before v. Consequently, the "plus" sign denotes moving of the target away from the radar.

According to the schematic of the experiment, the scattered signal (s^{sc}) is a time-delayed version of the incident signal (s^{in}) and is defined as:

$$s^{sc}(t) = A^{sc}(t)\cos(2\pi f^{sc} t + \varphi^{sc}),$$

where

$$\varphi^{sc} = \varphi^{in} - \frac{2\pi f^{in}}{c_0} 2R_0 \quad \text{and} \quad f^{sc} = f^{in} \mp f^{d} = f^{in} \mp f^{in}\left(\frac{2v}{c_0}\right) \tag{1.3}$$

Equation (1.3) introduces the theory of the Doppler Effect. The target, approaching or moving away from the radar, causes an increase or decrease of the received signal frequency (f^{sc}). The frequency (f^{d}) is called Doppler Shift and depends on the transmitted frequency (f^{in}) and the radar speed (v).

In the experiment presented in Figure 1.1, the Doppler frequency (f^{d}) is constant because the velocity (v) is also constant. In general, both the radar and the target change their spatial locations. They can also move in different directions having different non-constant velocities. In this case, the distance between the radar and the target is a non-linear function of time. The time derivative of R is used to define the Doppler frequency:

$$f^{d}(t) = \mp f^{in} \frac{2}{c_0} \frac{\partial R}{\partial t}$$

The output of the CW radar (s^{out}) is given as

$$s^{out}(t) = A(t)\cos\left(\pm 2\pi \int_0^t f^{d}(t)dt + \varphi\right) \tag{1.4}$$

As a consequence of equation (1.4), CW radars are unable to measure any range information from the target. The only information that can be derived from the measured signal (s) is the Doppler frequency (f^{d}) and amplitude (A).

The simple operational principles of CW radars allow their production using inexpensive components, which is the main reason that CW radars can be produced at low cost, thus making them attractive for NDT.

2. Experimental Setup

In order to perform experiments based on the Doppler Effect in microwaves, a prototype system has been developed and built. A prototype of this system is depicted in Figure 2.1.

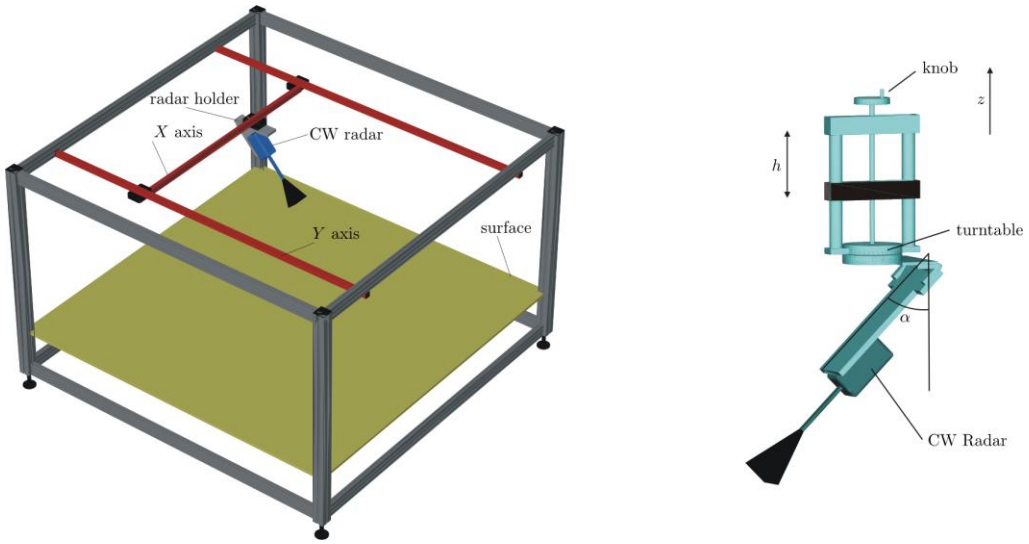

Figure 2.1: Prototype of the Doppler Measurement System

The CW Radar can move along the X and Y axis at a speed of up to 0.5 m/sec. The test object is placed on the surface located at the bottom of the system.

To adjust the spatial position and orientation of the radar, a radar fixture is used, see Figure 2.1. By using the radar fixture, the height of the radar (h) is adjusted by rotating the knob placed on top of the fixture. The range of the incident angle (α) can vary from 0 to 90 degrees. The radar fixture is equipped with scales for both h and α to allow for a precise adjustment of the CW radar. It is also possible to rotate the radar around the Z axis by using a turntable. This may be helpful if there is a need to change the direction of the scan. The motion of the X and Y axis is controlled from a PC. The motors driving the X and Y axis have an intelligent interface. Through this interface the motors can be programmed to execute a particular sequence of motions. While the radar is moving along the X or Y axis, the Doppler signals are acquired by a data acquisition board.

3. Experimental Results

3.1 Single Scan Amplitude Imaging

Let us consider a practical application of the Doppler Effect in microwaves applied for the characterization of wood. We performed surface scans on a number of wooden plates. Each surface was scanned line by line (from left to right) at an index of 3 mm. The surface images were generated by using the absolute value of the received Doppler amplitudes. Figure 3.1 present the results of the experiment. The photograph shows the visible knots in the wood grain. The knot size varies from about 2mm to 25mm in diameter. The Doppler image detected all knots except the one with a 2mm diameter. In addition, the experiment revealed the ability of the Doppler Effect to detect the texture of the wood plate, partially visible around the two largest knots.

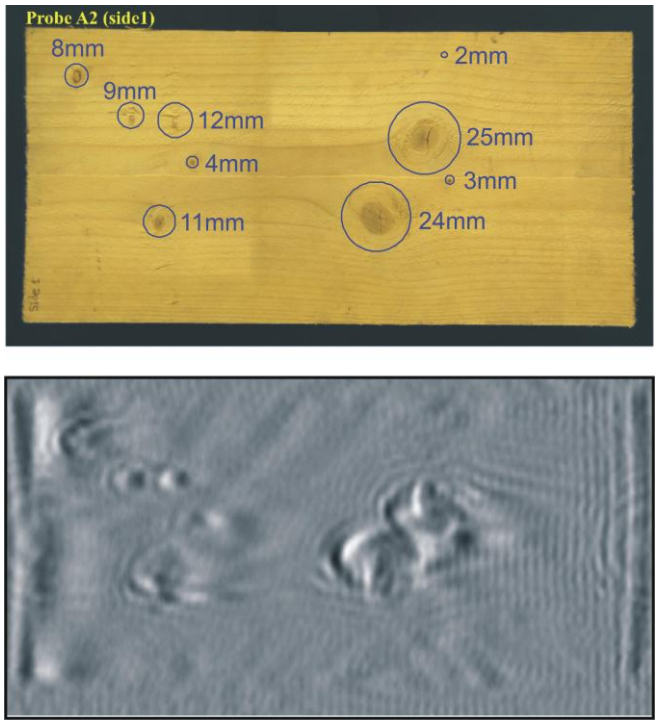

Figure 3.1: Scan of wooden plate

3.2 Multiple-Angle Doppler Imaging

The Doppler image of the specimen does not always display every discontinuity present. This is not caused by insufficient signal processing but rather by physical limitations. It occurs when the reflection from a flaw does not propagate back to the radar; this is the case when the discontinuity cannot be detected even if it is located inside the radar speckle.

In the following experiment, the Doppler image was acquired by a surface scan from left to right in the direction of the arrow (0 degrees scan) as shown in Figure 3.2(a). As shown in Figure 3.2(a), a circle made of a thin (1mm diameter) metal wire, was partially detected.

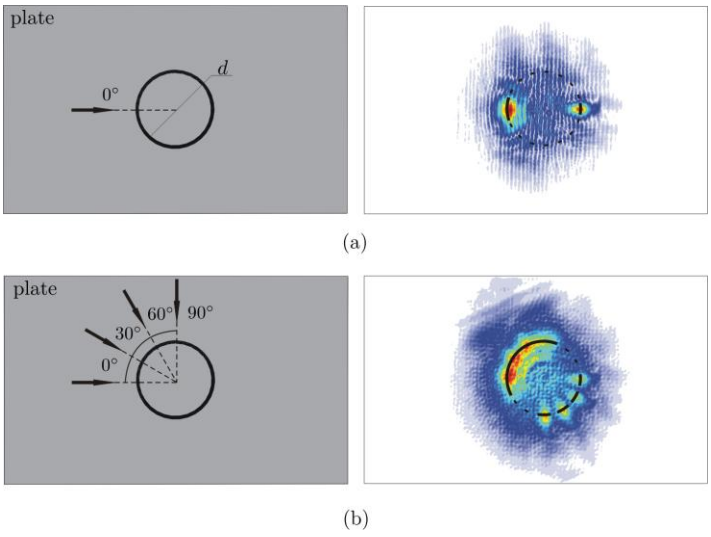

Figure 3.2: Multiple-angle Doppler Imaging of a Simple Geometry

The reflected signal only appears on the left and right edges of the circle, whereas the rest is not visible. To overcome this problem we proposed to perform Doppler imaging from

different view directions. This was achieved by rotating the sample around its center and scanning at 0, 30, 60 and 90 degrees. For every line in the measured image, the envelope was computed and the resulting images were arithmetically supplemented fto obtain a combined image. The resulting image is presented in Figure 3.2(b).

A multiple-angle Doppler imaging of a specimen presented in Figure 3.3(a) was performed on an aluminum plate with artificial flaws such as linear cracks and holes. The linear cracks were placed on the surface at incrementally increasing distances from 3mm to 45mm. The dimensions of the artificial linear cracks were: 100mm length, 6mm width and 6mm depth. The holes of the specimen had diameters varying from 3mm to 24mm in 3mm increments. The placement of the holes slightly deviated from the centerline.

Certainly, the distribution of the artificial flaws presented in Figure 3.3(a) does not represent actual flaw distribution. For example, it is unlikely that cracks (or other flaws) are nested closely to each other but are, in reality, rather spread over a larger surface. In this experiment, both artificial cracks and holes helped to investigate the spatial resolution ability of the Doppler image. Thus, the artificial cracks were used to determine the resolution in scan direction X. The holes were used to investigate the resolution ability in scan direction Y. Whether or not deviation of the hole distance from the centerline could be obtained in the resulting image was of special interest to us.

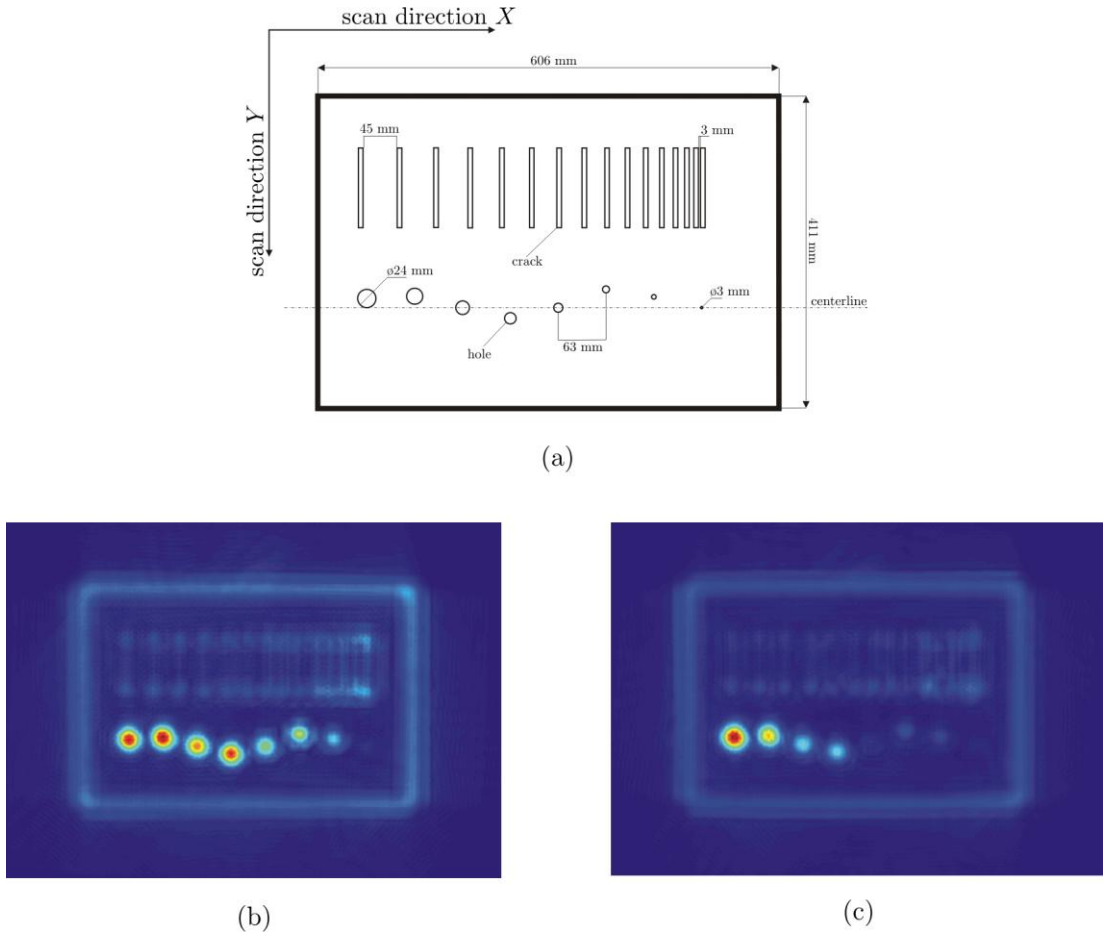

Figure 3.3: Multi-angle Doppler Imaging of an Artificial Specimen with and without Covering

The resulting image is presented in Figure 3.3(b). All holes except for the 3mm diameter hole were completely detected. The 3mm diameter hole was not detected because its size is below the radar detectability limit. The first six cracks (from left to right) were also well

recognizable, but it was difficult to separate the adjacent cracks (to the right); however the presence of flaws was still evident.

In the next step we performed a multiple-angle Doppler imaging of the same specimen covered with a semi-transparent material (PVC plate). The resulting image is presented in Figures 3.3(c). Here, disturbances and amplitude fading was caused by the PVC plate. Figure 3.3(c) demonstrates the significant quality degradation in comparison with the image in Figure 3.3(b). Nevertheless, in both cases (with and without plastic) almost all surface discontinuities are easily noticeable.

4. Theoretical Results

4.1 Maximum Entropy Deconvolution Algorithm

In general, the analysis of the Doppler amplitude does not allow a high spatial resolution to be achieved. To increase the spatial resolution the Maximum Entropy Deconvolution algorithm (MED) has to be applied. The idea behind MED is to find the solution of an n-dimensional maximization problem:

$$\max \quad -\left(S(\mathbf{x},\mathbf{b})+\alpha\cdot\chi(\mathbf{x},\mathbf{y},\mathbf{h},\sigma)\right)$$

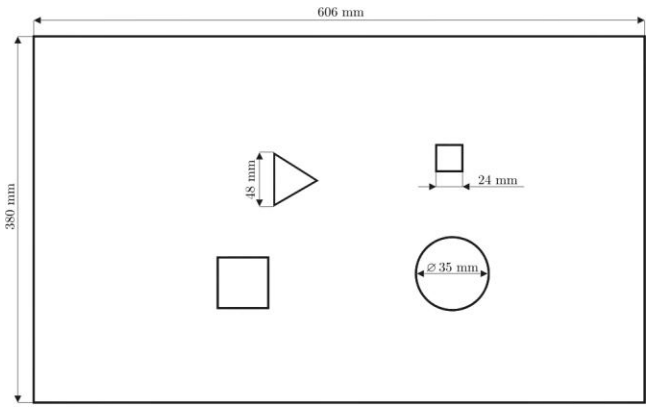

(a)

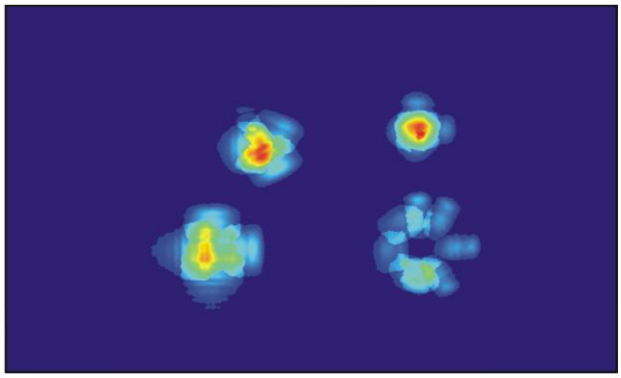

(b)

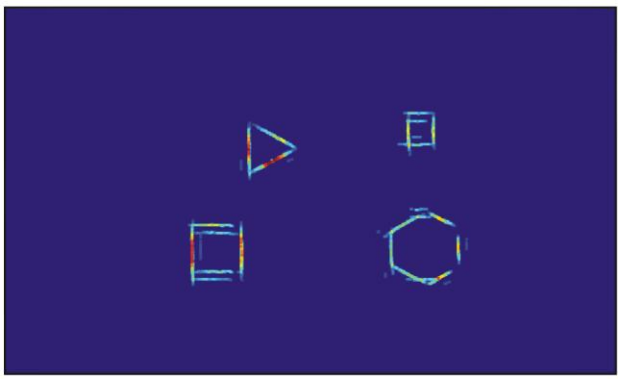

(c)

Figure 4.1: Maximum Entropy Deconvolution Results

where $\mathbf{x}, \mathbf{y}, \mathbf{z}$ represent characteristic signal, measured Doppler signal and an impulse response, respectively.
The functions S and χ are given as:

$$S(\mathbf{x},\mathbf{b}) = \sum_{i=0}^{n-1} x_i \left(\ln\left(\frac{x_i}{b_i}\right) - 1 \right) \quad \text{and} \quad \chi(\mathbf{x},\mathbf{h},\mathbf{y}) = \sum_{i=0}^{n-1} \frac{\left(y_i - (\mathbf{x} * \mathbf{h})_i\right)^2}{2\sigma^2}$$

The result of the experiment shows advantages of Doppler imaging based on the MED algorithm over amplitude Doppler imaging. To perform the experiment, a specimen as shown in Figure 4.1(a) was designed. The specimen consists of a rectangular metal plate with artificial flaws on the surface. The artificial flaws were made of metal wire (1mm

thickness) consisting of various geometrical shapes and sizes. Multiple-angle Doppler imaging was performed from several view angles. The measured surface scans were post-processed, rotated and merged.

The amplitude Doppler image is presented in Figure 4.1(b). Here, we can see a certain similarity to the specimen in Figure 4.1(a). Since the resolution ability of the Doppler amplitude approach is low, we cannot precisely determine the form of defects present. We can only determine the presence of defects and their locations. As we have discussed before, for many practical applications this may be the only requirement.

MED Doppler imaging provides significant resolution improvement. In Figure 4.1(c) the artificial flaws are separated and perfectly recognizable. By comparing Figures 4.1(a) and (c) we also conclude that the locations of detected indications entirely coincide with the artificial flaws within the specimen. The squared shape of the detected circle in Figure 4.1(c) can be explained by the small number of angle scans. In practice, it is unlikely to perform a large number of angle-scans and to precede the acquired data in a short time period.

4.2 Computational efficiency of the MED

In general, MED algorithm is computationally expensive. In order to increase the speed of computations we adapted its fast version for PC implementation. In Figure 4.2 we compare fast, conventional and hardware versions of the MED algorithm for different data lengths, namely 512, 1024, 2048, and 4096 samples. For all investigated data lengths the fast MED showed the best performance.

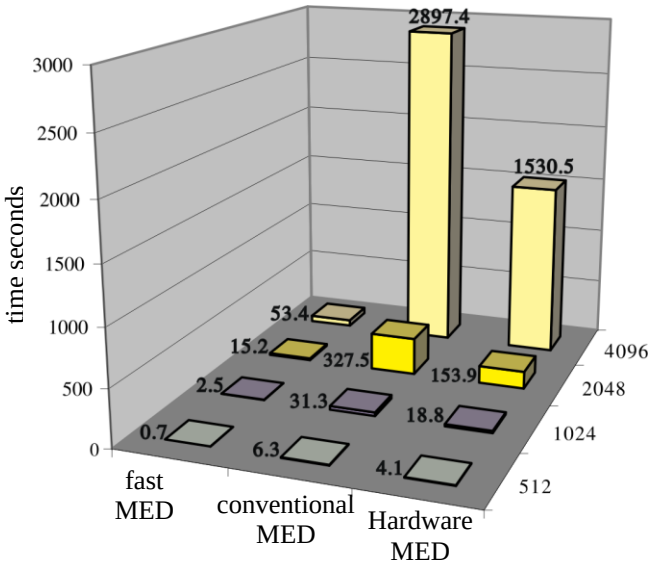

Figure 4.2: MED Computational Efficiency

5. Conclusion

We introduced a prototype of microwave Doppler system for Nondestructive Testing (NDT) purposes. This system satisfies the following requirements: inexpensive, easily integrated into industrial processes and fast measurements. It also includes software for hardware control, data acquisition and fast signal processing. The low cost of the Doppler system is achieved using continuous wave (CW) Doppler radars, which have become relatively inexpensive.

We suggested that a new type of 2D Doppler amplitude imaging should be developed and formalized. Such a technique is used to derive information about the measured object from several view angles. This imaging allows the user to detect most of the discontinuities included in the analyzed specimen.

The spatial resolution ability of CW radars was examined and improved. We have demonstrated that the MED algorithm can be used for the detection of pointed flaws and estimation of their exact spatial position. We also presented potential practical applications for the Doppler system.